Published in final edited form as:
Adv Biosyst. 2020 March 01; 4(3): e1900291. doi:10.1002/adbi.201900291.

In Vitro Platform for Studying Human Insulin Release Dynamics of Single Pancreatic Islet Microtissues at High Resolution

Dr. Patrick M. Misun[*],
Bio Engineering Laboratory Department of Biosystems Science and Engineering ETH Zürich Mattenstrasse 26, 4058 Basel, Switzerland

Dr. Burçak Yesildag[*],
InSphero AG Wagistrasse 27, 8952 Schlieren, Switzerland

Felix Forschler,
Bio Engineering Laboratory, Department of Biosystems Science and Engineering, ETH Zürich, Mattenstrasse 26, 4058 Basel, Switzerland

Aparna Neelakandhan,
InSphero AG Wagistrasse 27, 8952 Schlieren, Switzerland

Nassim Rousset,
Bio Engineering Laboratory, Department of Biosystems Science and Engineering, ETH Zürich, Mattenstrasse 26, 4058 Basel, Switzerland

Adelinn Biernath,
InSphero AG Wagistrasse 27, 8952 Schlieren, Switzerland

Prof. Andreas Hierlemann,
Bio Engineering Laboratory, Department of Biosystems Science and Engineering, ETH Zürich, Mattenstrasse 26, 4058 Basel, Switzerland

Dr. Olivier Frey
InSphero AG Wagistrasse 27, 8952 Schlieren, Switzerland

Abstract

Insulin is released from pancreatic islets in a biphasic and pulsatile manner in response to elevated glucose levels. This highly dynamic insulin release can be studied in vitro with islet perifusion assays. Herein, a novel platform to perform glucose-stimulated insulin secretion (GSIS) assays with single islets is presented for studying the dynamics of insulin release at high temporal resolution. A standardized human islet model is developed and a microfluidic hanging-drop-based perifusion system is engineered, which facilitates rapid glucose switching, minimal sample dilution, low analyte dispersion, and short sampling intervals. Human islet microtissues feature robust and long-term glucose responsiveness and demonstrate reproducible dynamic GSIS with a prominent first phase and a sustained, pulsatile second phase. Perifusion of single islet

patrick.misun@bsse.ethz.ch, burcak.yesildag@insphero.com.

Conflict of Interest
B.Y. and O.F. are members of the management team at InSphero AG, commercializing 3D microtissue solutions.

Europe PMC Funders Author Manuscripts

microtissues produces a higher peak secretion rate, higher secretion during the first and second phases of insulin release, as well as more defined pulsations during the second phase in comparison to perifusion of pooled islets. The developed platform enables to study compound effects on both phases of insulin secretion as shown with two classes of insulin secre-tagogs. It provides a new tool for studying physiologically relevant dynamic insulin secretion at comparably low sample-to-sample variation and high temporal resolution.

Keywords

diabetes; glucose-stimulated insulin secretion; hanging-drops; organ on chip; pancreatic islets

1 Introduction

Islets of Langerhans are the endocrine micro-organs of the pancreas that secrete a set of tightly regulated hormones that are fundamental to normal glucose homeostasis.[1] Pancreatic β-cells, the most common endocrine cell type of the islets, uniquely respond to changing blood glucose concentrations by secreting adequate amounts of insulin, the central hormone to normoglycemia. Relative or absolute deficiency in insulin results in diabetes mellitus, a group of heterogeneous disorders characterized by chronic hyperglycemia.[2]

Insulin release from pancreatic β-cells in response to glucose is a highly dynamic biphasic and pulsatile process.[3] Impairment of the dynamic insulin release can have a severe influence on glucose homeostasis and related physiological functions. Loss of the first phase, reduction of the second phase, and impairment of the oscillatory pattern of insulin secretion are, for example, characteristic features of type 2 diabetes (T2D) and contribute significantly to its progression.[3–5] Thus, studying dynamic insulin secretion is crucial for understanding the pathogenesis and pathophysiology of diabetes, as well as for assessment of pharmacokinetics and potential action mechanisms of anti-diabetic medication. Dynamics of insulin release, including the two phases and oscillations of glucose-stimulated insulin secretion (GSIS), can be investigated through time-resolved assay systems, such as pancreatic islet perifusion platforms. However, most commonly used perifusion platforms (e.g., Biorep Technologies, Miami Lakes, Florida)[6] require pooling of multiple islets per experimental condition in order to achieve quantifiable insulin concentrations and to tackle inherent variability in islet function. The pooling, in turn, entails a decreased resolution in dynamic insulin secretion due to the uncoordinated insulin secretion of individual islets, caused by the lack of input from the liver, pancreatic ganglia, and intestine that would normally synchronize individual islets in the body via glucose oscillations, neuronal input, and incretin secretion.[7–9]

Microfluidic platforms allow for manipulation of single cells and small cell aggregates, as well as precise control of small liquid volumes at the micrometer scale.[10–12] Therefore, they provide ideal means for miniaturizing islet perifusion systems. Previously reported microfluidic perifusion systems, developed to study dynamic insulin release from isolated pancreatic islets, rely on calcium imaging to measure the intracellular Ca^{2+} response,[13,14] on the collection of medium samples for biochemical analysis of secreted insulin[15–17] or

Europe PMC Funders Author Manuscripts

glucagon,[18] or on a combination of both, optical imaging and biochemical readouts.[19–22] However, the temporal resolution of the corresponding measurements is limited by the relatively large volumes in the majority of these devices, which preclude rapid liquid exchange and/or require pooling of multiple islets to achieve quantifiable insulin concentrations. The application of electro-osmotic flow and an online electrophoresis immunoassay,[23,24] along with miniaturization of the devices,[25–27] enabled researchers to resolve the highly dynamic and oscillatory secretion pattern of single islets.[28–30] However, the corresponding studies were almost exclusively based on rodent islets, which do not represent all aspects of the human organism. The only study that reports perifusion of single human islets does not seem to reproduce the physiological in vivo response of these micro-organs, as it includes only moderate increase in insulin secretion in response to glucose stimulation, no clear separation between the two phases of insulin secretion, and does not show realistic oscillations.[30] There are two potential reasons for the observed behavior; the heterogeneity of the native human islets and/or the compromised health of these islets following ex vivo culturing. Even within a single pancreas, islets display a striking variability in size—with diameters ranging from 50 to up to 500 μm.[31] Furthermore, islet cellular composition, especially in higher mammals, is highly heterogeneous.[32,33] For example, a human islet may include 28%–75% β-cells, 10%–65% α-cells, and 1.2%–22% δ-cells.[32] This natural variation makes it very difficult to obtain reliable and reproducible information using native islets, which becomes even more evident upon scaling down perifusion systems in order to measure the secretion dynamics of single islets. Therefore, the availability of homogenous islets can be considered a prerequisite to generate reproducible and reliable data sets with a reasonable sample size. Additionally, islets of insufficient purity —, i.e., including a large fraction of exocrine, nonislet tissue—may display fading functionality or rapid decline in viability. With unstable islet characteristics, the produced experimental data become highly dependent on the donor lot and the time point after isolation, which may compromise reproducibility and physiological relevance of the experimental outcome.[34]

In order to obtain uniform islet spheroids, isolated islets can be dissociated in primary-cell suspensions that feature physiological proportions of the various islet endocrine cell types, and the dissociated cells can then be reaggregated in controlled ratios.[35–38] However, the formation of human pseudoislets featuring physiological GSIS response remains challenging. A recent study compared GSIS data, obtained with pooled fresh and cultured native islets, to those obtained with pooled pseudoislets, generated in low-attachment wells. The results evidenced that the pseudoislets performed better in comparison to cultured native islets; however, they also have limitations in fully reproducing the physiological two-phase secretion response of fresh native human islets.[34]

Finally, other reasons for the low number of reports on microfluidic perifusion systems and dynamic GSIS information may include the complexity of experimental setups, which limits reproducibility and prevents the adoption of microfluidic systems by a larger community. Required system features include: (i) simple loading and precise positioning of single islets in a miniaturized and perfused culturing compartment; (ii) precise fluid control with an optimal flow profile to minimize delays, dispersion, and dilution of secretory products; and (iii) high sampling rate in combination with a standard analysis method.

In an effort to cope with all the issues mentioned above, we developed an analytical platform, including (i) a microfluidic hanging-drop-based perifusion system and (ii) a uniform islet microtissue model. The reaggregated primary islet model featured representative and homogeneous size and native-like distribution of endocrine cells within each aggregate, as well as physiologically relevant beta cell function. The microfluidic system design is based on the hanging-drop technology.[39–45] Single islets were loaded into and inherently placed at the bottom of a hanging-drop. Microfluidic hanging-drops provide precise perifusion control due to the minimal dead volume, fast liquid exchange, and operational simplicity, while islet viability is maintained through sufficient oxygen supply in the open system. By combining the uniform and highly functional islet microtissues with the miniaturized, completely open microfluidic chip design and by using high liquid-sampling rates, we were, for the first time, able to resolve the characteristic dynamic insulin release features of single human islets. These characteristic features included a pronounced first phase and distinct oscillations in the second phase. We studied two different classes of insulin secretagogs, exendin-4 and tolbutamide, to demonstrate how the newly developed platform could be used to assess compound effects on the dynamic insulin release patterns.

2 Results

2.1 The Standardized Pancreatic Islet Model—Human Islet Microtissues

The experimental use of isolated native islets has multiple limitations due to their inherent heterogeneity in size and function, varying endocrine cell composition, and low purity. Additionally, quickly after isolation, islets decline in viability and functionality with regard to their glucose responsiveness.[46,47] It has long been known that dissociated isolated islets can spontaneously reaggregate into islet-like clusters, with native-like architecture and secretory function.[37,48–50] The reaggregation process also provides control over the islet size, which enables the generation of smaller islets. The smaller islets display stronger GSIS in perifusion assays and more favorable glycemic outcomes after transplantation in vivo.[51,52]

Islet microtissues were produced by enzymatic dissociation and controlled scaffold-free hanging-drop-based reaggregation of primary islet cells to obtain a standardized islet size[31] of around 150 μm, which is a representative number for the average islet size in a human isolate[38] (**Figure 1a**). The resulting uniform islet microtissues are cultured in a one-islet-per-well format in 3D-cell-culture-optimized 96-well microwell plates (Akura 96, InSphero AG). Immunostaining for the most common endocrine cell types of pancreatic islets; the insulin expressing beta (β) cells, the glucagon expressing alpha (α) cells, and the somatostatin expressing delta (δ) cells revealed that islets microtissues have a composition, which closely resembles that of the human pancreas[53] (52.9% β-cells, 36.7% α-cells, and 7.7% δ-cells) (Figure 1b). The islet size was reproducible over several aggregations (Figure 1c), and microtissues featured sustained viability (indicated by the total adenosine triphosphate (ATP) content; Figure 1d) during 28 d in culture. The insulin content, on the other hand, increased with culture time (Figure 1e). Throughout these 4 weeks, islet microtissues also displayed robust GSIS as evidenced by microtissues from seven different donors reaching an average of 15.7-fold higher insulin release at 16.7×10^{-3} M glucose

concentration compared to the release at 2.8×10^{-3} M glucose at day 28 (Figure 1f). Following the reaggregation process, we observed moderate donor-to-donor variations in beta cell function (Figure 1g). Out of the 15 donors tested, the maximum difference in stimulated insulin secretion in response to 16.7×10^{-3} M glucose was 2.8-fold (between donors 11 and 14), and the maximum difference in the basal insulin secretion rates was 4.1-fold (between donors 4 and 8). More variation was apparent at intermediate glucose concentrations. For example, insulin secretion response to 5.5×10^{-3} M glucose exhibited an eightfold difference between donors 4 and 5.

2.2 The Microfluidic Perifusion System

The microfluidic hanging-drop chip was designed as an open microfluidic system.[41–45] **Figure 2a** displays the layout and dimensions of the chip in a top view, while cross-sectional views are shown in Figure 2b and Figure S1a (Supporting Information). Due to surface tension and capillary action, small liquid volumes can be guided underneath the surface-patterned poly(dimethylsiloxane) (PDMS) substrate.

The loading procedure of the chip is simple and short. A single microtissue is directly loaded with a small liquid volume into the empty drop structure, until a small standing drop is formed. The chip is then flipped upside down to let the microtissue sediment to the bottom of the hanging-drop and is afterward placed on a microscope stage using a dedicated holder.

Figure 2b shows the microfluidic setup from the side. Three syringe pumps with different media are connected via adapters to the inlets of the chip and operated according to a predefined perifusion script. Inflow rates of the syringe pumps were set to 15 μL min^{-1}. A peristaltic pump was set to withdraw medium from the outlet at a constant rate of 15 μL min^{-1}. An automated sampling system was used to collect medium samples into a 384-well plate. The medium flow caused a maximum shear stress of 1.81 mPa on the islet microtissue, when a flow rate of 15 μL min^{-1} was applied (Figure S1b, Supporting Information).

A trade-off between flow rate (dilution of secreted insulin) and minimal required sampling volume for enzyme-linked immunosorbent assay (ELISA) defined the sampling frequency. The flow rate was optimized to reduce the dilution of secreted insulin so that it remained above the limit of detection of the ELISA (2 pg mL^{-1}) and to maximize the sampling frequency. A minimum volume of 5 μL is required to prepare the ELISA samples, which limits the sampling rate to three samples per minute when applying a flow rate of 15 μL min^{-1}. Combining the automated sampling system with a flow-rate controller ensured consistent sampling volumes, stable flow rates, and steady drop sizes throughout the experiment (Figure S1c, Supporting Information).

The hanging-drop was used as a miniaturized microtissue culturing compartment with a volume of 6.5 μL (Figure S1a, Supporting Information). The microfluidic chip did not have any dead volume, and the completely open chip design reduced the PDMS surface area in contact with the liquid phase, which lowered the risk of analyte ad/absorption in PDMS. The open hanging-drop chip design ensured sufficient oxygenation of the medium and prevented bubble formation in the chip. The effect of gravity and the low flow speed at the islet site

ensured stable positioning of the cultured islet microtissue at the bottom of the hanging-drop and obviated the need for trapping structures. The precise and stable location of the microtissue at the bottom of the drop also ensured identical flow conditions in every experiment, which increases reproducibility. Finally, the hanging-drop features a characteristic flow profile and a rapid and efficient medium exchange around the microtissue (Figure 2c).

We measured the dynamics of the medium exchange in the hanging-drop by switching from deionized water to a fluorescent dye (Rhodamine 6G) and then back to deionized water (Figure S1d, Supporting Information). We simulated the dynamics by implementing a numerical model (details in the Supporting Information) yielding average concentrations of Rhodamine 6G—both in the hanging-drop and around the islet microtissue—that we compared to the experimental relative fluorescence data (Figure 2c). The medium exchange time—defined as time to go from 5% to 95% analyte fraction—amounted to 89 s in the hanging-drop, with a good fit between model (dotted black line) and experiments (red line), and to 13 s in the region around the islet microtissue (black line). The discrepancy between experiment and simulation for the step increase in fluorescence can be explained by a slower absorption of Rhodamine 6G by PDMS than expected.[54] Nevertheless, the fit between experiment and simulation allowed us to affirm that medium switching near the microtissue happens 5.8 times faster than observed across the drop. Therefore, medium switching at the microtissue is faster than the insulin sampling rate of 30 s, which enables a precise timing of the glucose stimulation of pancreatic islets.

The hanging-drop setup has an additional advantage over more conventional closed microfluidic devices. The air–liquid interface near the secreting organ exhibits a slip boundary that enables to transport metabolites more rapidly than the no-slip boundary of closed microfluidic devices. This enables resolving much sharper changes in the secretion dynamics. To demonstrate this feature, a sharp 1-s-wide insulin secretion burst at the pancreatic islet was simulated (Figure 2d). The results show that, with the slip boundary, one can detect this sharp peak within one 30 s sample, whereas with a no-slip boundary the true signal from the islet is widened five times (for comparison we assumed a bottom-closed system with the same channel and compartments). Sampling that is in-phase and out-of-phase of a secretion event is shown in Figure S2a,b (Supporting Information). The simulations show that we can resolve insulin oscillations down to a frequency of one cycle per min, if we sample in phase, and down to 0.5 cycles per min, if we sample out of phase. Consequently, the measurements will not provide any additional information about the dynamics of secretion events in time spans shorter than the sampling interval of 30 s. Numerical modeling results of the concentrations through the chip along a cross section demonstrate the transport characteristics of secreted insulin within the hanging-drop (Movie S3, Supporting Information).

2.3 Insights in Islet Secretion Dynamics, Mechanistic Function, and Biology of Single Islets

The physiological release of insulin from healthy β-cells in response to glucose is highly dynamic and results in a characteristic biphasic and pulsatile insulin secretion pattern.[3] The

robust first phase of the biphasic insulin secretion is mediated by the limited readily releasable pool of insulin granules, which are associated with the cell membrane.[55] The second phase of GSIS is sustained by the granules that are transported from the intracellular reserves.[55]

We used an on-chip microfluidics-based glucose-stimulated insulin secretion protocol (FlowGSIS) with precise timing and sampling to characterize the secretion dynamics of single human islet microtissues. A glucose enriched Krebs–Ringer buffer was constantly perfused at a flow rate of 15 μL min^{-1}. Glucose concentration was first kept low at 2.8 × 10^{-3} M for 105 min and then switched to high 16.7 × 10^{-3} M for 60 min before switching back to 2.8 × 10^{-3} M for 60 min. The low liquid volume minimized dilution effects of secreted hormones and allowed for a sampling every 30 s.

Figure 3a shows an exemplary curve with a typical insulin secretion pattern of a single islet microtissue. During the initial phase, basal secretion values are constant and show low variation along the time axis with a standard deviation of ± 0.05 fmol IEQ^{-1} min^{-1} proving good reproducibility between samples. A fast increase in glucose concentration from 2.8 to 16.7 × 10^{-3} M glucose induced a reproducible biphasic insulin secretion pattern with a prominent first phase and a sustained, pulsatile second phase. The observed oscillatory secretion of insulin indicated an intact intercellular communication and a synchronized release of insulin from the β-cells present in the islet microtissues.

Figure 3b,c shows parameters of dynamic insulin release, which were extracted from single-islet-microtissue perifusion experiments including insulin secretion rates in different phases, the peak secretion rate, timing of insulin release, and the total secreted insulin during a full GSIS assay. The full set of parameters that can be extracted from such a FlowGSIS assay is listed in Table S4 (Supporting Information).

In the presented case, the basal insulin secretion from a single islet microtissue was 0.25 fmol IEQ^{-1} min^{-1} for low glucose (2.8 × 10^{-3} M). Interestingly, we repeatedly observed a short (≈3 min) but distinct dip in insulin secretion when switching to high glucose (16.7 × 10^{-3} M) prior to the start of the first phase in which the secretion rates reached rapidly 7.0 fmol IEQ^{-1} min^{-1} within 2.5 min. This prominent first peak lasted for 8 min. In the second phase, we observed pulsatile insulin secretion with a 5.5 min period for 20 min, followed by prolonged 11 min period for 40 min. Peaks of insulin secretion decreased from 5.0 to 1.5 fmol $IEQ^{-1}min^{-1}$ through this pulsatile phase. Prolonged low frequency, pulsatile secretion lasted for 15 min after switching back to low glucose medium (2.8 × 10^{-3} M).

Figure 3b shows the average secretion rates and the distribution of insulin release in all different phases of the Flow-GSIS represented in Figure 3a. Clearly, the highest secretion rate occurs during the first phase with a total insulin release of 31.9 fmol. In the second phase, the insulin secretion rate drops significantly but remains relatively stable. The total secreted insulin in this second phase depends on the duration of the high-glucose phase, and, thus, is only comparable, if the high-glucose phase duration time is kept constant between experiments. The respective measurements of islets from different donors are shown in Figures S5 and S6 (Supporting Information).

Figure 3c presents timing and duration of every phase of the FlowGSIS assay. Islets across different donors show a very precise timing and respond reproducibly to high glucose stimulation. Islets responded in average within 4.6 ± 1.0 min (t_{Response}) to high glucose levels reaching a peak secretion rate of 11.2 ± 6.6 fmol IEQ^{-1} min^{-1} in the first phase within 3.6 ± 0.8 min (t_{Peak}). The first phase (t_{Ph1}) lasted a total of 9.9 ± 1.4 min. Islets showed a delayed response after switching to low glucose levels, with a relaxation time ($t_{\text{Relaxation}}$) of 19.7 ± 11.1 min. The response time, the time to reach peak secretion, and the duration of the first phase were particularly reproducible over different donors, whereas the peak secretion rate and relaxation time showed higher variations across islets from different donors.

Compared to the standard static GSIS, the mean secretion rate over both high-glucose phases is in average 7.6-fold higher in the perifusion system (4.0 ± 3.1 fmol IEQ^{-1} min^{-1} in the FlowGSIS compared to 0.5 ± 0.4 fmol IEQ^{-1} min^{-1} in the static GSIS). However, the stimulation-level factor from average basal secretion at 2.8 × 10^{-3} M glucose to the average secretion at high glucose levels (16.7 × 10^{-3} M) remains the same under both, static (16.0 ± 8.9) and FlowGSIS conditions (15.4 ± 10.1) (Figure 3d).

2.4 The Islets Recapitulate In Vivo Compound Response

Insulin secretagogues are antidiabetic medication that aims at increasing the insulin output of pancreatic islets. In order to verify whether the assay platform can be used to study compound-stimulation mechanisms for insulin secretion, we have treated the islet microtissues with two different classes of insulin secretagogues: tolbutamide, a sulfonylurea-class compound, and exendin-4, a glucagon-like-peptide-1 receptor (GLP-1R) agonist.

Sulfonylureas are the most commonly prescribed insulin secretagogues due to their high efficacy, wide availability, and low costs.[56] However, their administration entails a significantly increased risk of hypoglycemia due to a potential increase in insulin levels at low circulating glucose concentrations.[56] The effect of sulfonylureas (e.g., tolbutamide) is based on blocking the ATP-sensitive K^+ channels on the surface of pancreatic beta cells, which leads, through a chain of events, to a rise in intracellular calcium levels.[57] Elevated calcium levels result in increased fusion of insulin granules and higher levels of insulin secretion (even under low levels of glucose).[57]

In the static GSIS experiments, addition of tolbutamide resulted in a substantial increase in insulin secretion for all tested glucose concentrations (**Figure 4a**). The secretion rate was increased by 0.21–0.37 fmol IEQ^{-1} min^{-1} from 2.8 to 8.0 × 10^{-3} M glucose in comparison to the vehicle control and remained constant at 0.68 fmol IEQ^{-1} min^{-1} from 8.0 to 16.7 × 10^{-3} M glucose.

Similarly, tolbutamide increased basal insulin secretion at 2.8 × 10^{-3} M glucose in the high-resolution FlowGSIS experiment (Figure 4b). Tolbutamide increased the baseline secretion rate at 2.8 × 10^{-3} M glucose from 0.16 to 0.89 fmol IEQ^{-1} min^{-1} and caused a partial attenuation of the following first phase of GSIS from 7.1 to 5.1 fmol IEQ^{-1} min^{-1} (maximum secretion rate) in comparison to the vehicle control. The total amount of glucose-stimulated insulin release in the second phase was comparable for the first 30 min (140–170 min) for tolbutamide (42.1 fmol insulin) and solvent-only treated islets (41.3 fmol insulin).

However, addition of tolbutamide helped to sustain higher levels of insulin secretion for elongated exposure (170– 195 min) to high glucose levels (tolbutamide: 41.8 fmol insulin; vehicle control: 18.7 fmol insulin).

Next, we tested the effects of GLP-1R agonists, another well-established and clinically used class of insulin secretagogs, on the dynamic insulin secretion of islet microtissues. GLP-1 is an incretin hormone that is naturally secreted from the intestinal L-cells in response to elevated glucose concentrations. It activates the GLP-1Rs on the pancreatic β-cells,[58] which, in turn, increase insulin secretion through multiple glucose-initiated events.[58] Owing to their glucose-concentration-dependent mechanism of action, GLP-1R agonists represent a safer option for hypoglycemia.[59]

As expected, in the static GSIS experiments, addition of exendin-4 potentiated insulin secretion in a glucose-dependent manner (Figure 4c). The first small—but significant—increase in insulin secretion was observed at 5.5×10^{-3} M glucose with increasing effects at higher glucose concentrations, e.g., from 0.40 to 0.91 fmol IEQ^{-1} min^{-1} at 16.7×10^{-3} M glucose.

Similarly, addition of exendin-4 did not influence basal insulin secretion at 2.8×10^{-3} M glucose in the FlowGSIS experiments (Figure 4d). During this prestimulation phase (80–110 min) the total secreted insulin was in average 3.5 fmol in the vehicle control and 4.0 fmol for exendin-4. An increase in GSIS was mostly present in the second phase (120–180 min). The total secreted insulin was on average 83.7 fmol in the vehicle control and 128.0 fmol for exendin-4.

2.5 Comparing Static and FlowGSIS

The measurements in Figure 4 show that islets in the perfused hanging-drop secrete insulin at higher rates compared to the static well plate condition. The baseline secretion of untreated islets under static conditions is 0.01 fmol IEQ^{-1} min^{-1} at 2.8×10^{-3} M glucose and 0.40 fmol IEQ^{-1} min^{-1} at 16.7×10^{-3} M glucose. Untreated islets under perfused conditions secrete insulin at an average rate of 0.13 and 1.56 fmol IEQ^{-1} min^{-1} at 2.8×10^{-3} M and 16.7×10^{-3} M glucose, respectively. Tolbutamide and exendin-4 increased insulin secretion under perifusion in the high-glucose phase to 1.65 fmol IEQ^{-1} min^{-1} and 2.30 fmol IEQ^{-1} min^{-1}, respectively. Figure S8 (Supporting Information) shows that the ATP content of islets was not affected by the compounds for concentrations of 25×10^{-6} M tolbutamide, 100×10^{-9} M exendin-4, and 0.1% dimethyl sulfoxide (DMSO) as the vehicle control.

2.6 Compounds Influence Mechanistic Parameters

Exendin-4 and tolbutamide altered the dynamics of insulin release of islets in FlowGSIS assays. We analyzed the data by looking at characteristic parameters, which we extracted from the high-resolution FlowGSIS measurements to get more insights into how both compounds change the insulin secretion pattern of islets.

Figure 5a describes and compares the distribution of secreted insulin over all phases of insulin release during Flow-GSIS. It shows the amount of insulin that was secreted in each

phase relative to the total secreted insulin of the overall FlowGSIS. This analysis provides information about the shape of the GSIS curve and it shows how compounds change this characteristic insulin release pattern. In general, insulin was predominantly released during the high-glucose phase (first phase and second phase). The baseline secretion is similar for all the samples. Tolbutamide increased insulin release in the prestimulation phase and in the poststimulation phase at low glucose levels (2.8×10^{-3} M).The early release of insulin in the prestimulation phase reduced insulin release in the high-glucose phase (16.7×10^{-3} M), which was especially pronounced in the second phase. This shows that tolbutamide altered the dynamics of insulin release during GSIS, whereas exendin-4 did not change the shape of the insulin secretion curves in comparison to the control. The total amount of secreted insulin in all phases depends on the duration and timing of the low and high glucose conditions in the GSIS.

Figure 5b shows how exendin-4 and tolbutamide affect the insulin secretion rate in each phase of the FlowGSIS. Tolbutamide increased the secretion rate of insulin at low glucose (2.8×10^{-3} M) concentrations—the prestimulation phase—12.9 ± 7.7 fold, and in the poststimulation phase 3.67 ± 3.32 fold. The peak secretion rate and the secretion rate during high-glucose phases (predominantly first phase) were reduced by 0.72 ± 0.01 fold and 0.84 ± 0.26 fold, respectively. Exendin-4 had no effect on the secretion rate in the prestimulation phase (1.12 ± 0.29 fold change). The peak secretion and the first phase were not affected (0.93 ± 0.11 and 0.94 ± 0.04 fold change). Exendin-4 increased the insulin secretion rate in the high-glucose phase (predominantly second phase) 1.53 ± 0.16 fold, and reduced the secretion in the poststimulation phase 0.57 ± 0.27 fold.

Figure 5c describes how both compounds affect the timing of insulin release during FlowGSIS relative to the control. The response time (t_{Respons}e, exendin-4: 0.85 ± 0.31 fold change; tolbutamide: 0.98 ± 0.21 fold change) and the duration of the first phase (t_{Ph1}, exendin-4: 0.92 ± 0.04 fold change; 0.91 ± 0.10 fold change) were not affected by the compounds, whereas exendin-4 reduced (0.70 ± 0.42 fold change) and tolbutamide increased (1.23 ± 0.61 fold change) the time to reach peak secretion (t_{peak}). Exendin-4 had no effect on the relaxation time (t_{Relaxa}t$_{\text{ion}}$) (0.97 ± 0.04 fold change), whereas tolbutamide largely extended this phase (2.85 ± 1.83 fold change).

2.7 Perifusion of Islet Pools Leads to Loss of GSIS Resolution

Finally, we assessed the effect of pooling multiple islets on the temporal resolution of the perifusion studies. For this purpose, we perifused either single islet microtissues or a pool of three islet microtissues from the same donor. While perifusion of a single islet microtissue enabled detection of very distinct and reproducible pulsations, we could not observe clear oscillations, when multiple islet microtissues were pooled in one perifusion chamber (**Figure 6**). This was most likely a result of the averaging of asynchronous insulin secretion patterns of the individual islets. Pooling of multiple islet microtissues in the perifusion system also resulted in a reduced peak secretion, blunting of the first phase, and a reduced secretion in the second phase, which substantiates the importance of conducting single-islet perifusion studies (Figure 6). Nevertheless, the dosage of exendin-4 increased GSIS for both, single and pooled islet perifusions (control in Figure 6a and exendin-4 in Figure 6b).

Europe PMC Funders Author Manuscripts

3 Discussion and Conclusions

Growing evidence suggests that a loss of the first-phase insulin response or a pulsatile insulin secretion is not only characteristic feature of T2D but also contributes significantly to its etiology.[4,5] Restoration of the early phase insulin response and the subsequent oscillations have been shown to improve blood-glucose levels in T2D patients and, therefore, constitute important therapeutic measures.[60,61] However, it is very challenging to obtain physiologically relevant outcomes from in vitro dynamic insulin-secretion studies, especially with human islets. Here, we show that this challenge may be partially due to the use of islet pools, which entails the loss of experimental resolution—such as blunting the secretion peak in the first phase or averaging the oscillations in the second phase. The use of single-islet perifusion systems is, therefore, better suited to study time-resolved insulin secretion, but the consistency of results may suffer from the variability in size, composition, and health of native rodent and human islets.[23,30] Furthermore, even if single-islet perifusion systems are better suited to study time-resolved insulin secretion, existing systems have issues or limitations including the complexity of experimental setups, the adsorption of analytes at walls and surfaces of fluidic structures, the large dilution and dispersion of secreted molecules and compounds, the increased shear stress on the islets, and the lack of oxygen during longer time stretches.

Our approach to address the challenges listed above includes a combination of a microfluidic hanging-drop perifusion system with a standardized and highly functional human islet model. This approach enabled us to measure the native biphasic, pulsatile, and oscillatory insulin release of single reaggregated primary human islet microtissues. In every assay that we performed, we reproducibly saw a pronounced first phase and a sustained pulsatile second phase, as well as clear boundary between these two phases of insulin secretion. The high measurement success rate is due to the tissue quality and the technical features of the platform.

Our human-derived reaggregated islet microtissues provide a decisive advantage over native islets, as they featured homogenous and robust insulin secretion, while they retained viability and physiological GSIS responses over 4 weeks. The uniformity and reproducibility of the secretion curves, which is especially pronounced in islets from an individual donor, enabled experimentation with significantly smaller sample sizes for the assessment of compound effects in comparison to previous studies.[23,30] The perifusion experiments evidenced the high functionality of the human-derived islet microtissues, e.g., through a 35-fold increase in insulin secretion during the first phase and a 64-fold stimulation from basal to peak secretion. Additionally, the sharp oscillations in the second phase of insulin secretion indicate robust cellular communication throughout the reaggregated islets resulting in functional synchronization of the beta cells.[53] These measurements show that our pancreatic human islet model can be considered a relevant in vitro model system, as it closely recapitulates the physiological response of current native islets in vitro[34] and in vivo.[62,63]

The microfluidic hanging-drop perifusion system enabled us to thoroughly characterize insulin release from single islets by extracting distinct dynamic parameters. Islets under

perifusion had higher secretion rates of insulin compared to static conditions; however, the proportions between basal insulin secretion and GSIS remained unchanged. One of the factors causing higher secretion rates in the flow system could include that there is, due to the flow, no local accumulation of somatostatin, which would inhibit insulin secretion.[64] Characteristic time points of the GSIS, especially the initial response time, the time to reach peak secretion, and the duration of the first phase were well preserved across different donor islets, whereas the average secretion rates, the peak secretion rate, the relaxation time, and the frequency and the intensity of the oscillations showed higher variability across donors.

Moreover, we performed proof-of-concept studies for pharmacological manipulation of islet function in order to display how our platform can enable the investigation of how different compounds alter the insulin-secretion dynamics. Compared to a standard GSIS, performed in static setups within multi-well plates, the results obtained under perifusion enable more detailed characterization and assignment of compound-related stimulation effects in the respective secretion phases. We observed that continuous tolbutamide treatment at low and high glucose levels resulted in a pronounced increase in basal insulin secretion. This increase in the basal secretion rate could pose a risk for severe hypoglycemia[56] and, therefore, is an unfavorable characteristic of an insulin secretagog. We also observed that a sulfonylurea-mediated increase in the basal secretion could lead to blunting of the first phase of stimulated insulin secretion, which confirms the importance of the treatment timing using sulfonylureas, e.g., right before meals. A potential reason for the blunting of the first phase may be an early exhaustion of the readily releasable pool of insulin granules. On the other hand, exendin-4's actions were glucose-level-dependent, and exendin-4 only potentiated stimulated glucose secretion. This characteristic of GLP-1R agonists renders them a safer class of compounds with regard to hypoglycemia.[65] We observed that exendin-4 stimulated insulin secretion, most pronouncedly the second phase with sustained oscillations. Our results indicate that the presented platform could be employed to study important parameters for estimating drug efficacy and safety.

On the technical side, the use of a completely open microfluidic chip design with the hanging-drop technology enabled precise fluid control with short delays. The characteristic flow profile in hanging-drops helped to minimize dispersion effects and sample dilution, which typically arise in closed microfluidic systems. The use of hanging-drops in the perifusion system facilitated rapid medium switches and short sampling intervals, which, in turn, enabled us to resolve details of the insulin secretion dynamics of single-islet microtissues. Moreover, the open microfluidic chip design obviated bubble formation and helped to reduce the surface area of the PDMS substrate, which decreased analyte surface adsorption and bulk absorption.[66] The newly engineered system has proven to be very robust, it is simple to set up and operate. Islet microtissues could be conveniently loaded and retrieved from the hanging-drop perifusion chamber. They experienced stable flow conditions during the experiments, which promoted measurement reproducibility. The position of the islets at the liquid–air interface also helped to preserve their morphology and ensured continuous oxygen supply, which is essential to maintain islet functionality and viability in vitro.[67–71] Moreover, the microtissue position at the largest cross-section of the fluidic duct and the open chip design with its characteristic slip boundary condition at the

Europe PMC Funders Author Manuscripts

air–liquid interface helped to minimize flow-induced shear stress on the microtissue and ensured rapid liquid turnover.

Consequently, our approach represents a novel method to study time-resolved insulin secretion from a primary human islet model that closely and reproducibly recapitulates physiologically relevant responses to glucose, thereby enabling efficient pharmacological studies with a small number of technical replicates. The presented platform constitutes a promising tool for the discovery of novel mechanisms or compounds that would restore first-phase or oscillatory insulin secretion of diabetic human islets, as it provides the resolution that is required for such analyses.

4 Experimental Section

Reaggregated Human Islets

InSphero 3D InSight human islet microtissues were produced by hanging-drop-based scaffold-free reaggregation of dispersed primary human islets obtained through Prodo Laboratories Inc. Irvine, CA. Consent was obtained from all next of kin, and there was no information on the identity of the donor for ethical and privacy reasons. For each production, between 10 000 and 20 000 islet equivalents (IEQs) were dispersed in dissociation solution (1992 µL TrypLE Express (1X) solution plus 8 µL DNase I, 10 mg mL^{-1}, to a final concentration of 40 µg mL^{-1}) by gentle pipetting at 37 °C. Remaining cell clumps were removed by filtering the cell suspension through a cell strainer (70 µm pore size). Two thousand and five hundred cells were seeded into each well of the InSphero Hanging Drop System and cultured for 5 d according to manufacturer's instructions. The primary aggregates were then transferred to the Akura 96 well-plate to further mature for at least another 8 d before the start of the experiments. All experiments were performed 14–28 d after the start of the aggregation. Islet microtissues were maintained in 3D InSight Human Islet Maintenance Medium (InSphero AG, Schlieren, Switzerland).

Microfluidic Hanging-Drop Chip Fabrication

Microfluidic chips were fabricated using a SU-8 mold and casting PDMS (Sylgard 184, Dow Corning GmbH, Wiesbaden, Germany).[72] A 4 in. silicon wafer was used as a substrate in a multi-layer photolithographic process. The wafer was consecutively spin-coated with two layers of negative photoresist SU-8 100 (Microchem Corp., Newton, MA, USA) at a thickness of 250 µm for each layer. The wafer was soft-baked after deposition of each layer and UV exposed through a transparency mask for crosslinking. A postexposure baking step followed for each layer. The wafer was developed in mr-Dev 600 (Micro resist technology GmbH, Berlin, Germany) to dissolve all unexposed SU-8 and afterward coated with trichloro(1H,1H,2H,2H-per-fluorooctyl)silane (Sigma-Aldrich, Buchs, Switzerland) to reduce adhesion during PDMS casting.

PDMS was prepared by mixing the elastomer and curing agent in a 10:1 ratio. PDMS was poured onto the SU-8 mold resulting in a 3 mm thick layer and cured for 2 h at 80 °C. Individual chips were cut, and access holes were punched on the outlet and inlet side for the

fluidic connection. Finally, the PDMS chip was bonded to a microscope slide featuring corresponding access holes by oxygen plasma activation of both parts.

Device Preparation

The microfluidic chip was cleaned with water and soap, rinsed with isopropanol, and dried with pressurized air. The microfluidic structures were treated with oxygen plasma for 35 s at 50 W (Diener Electronic GmbH & Co., Ebhausen, Germany) before any experiment to obtain a hydrophilic surface. Therefore, a thin PDMS mask with a small opening at the drop position was aligned to the hanging-drop chip. The mask covered the rim and allowed to activate only the drop structure and channels through the oxygen plasma. The activated hanging-drop chip was placed on a custom-made chip holder, which fits into a Nunc OmniTrayBox (Thermo Fisher Scientific, Reinach, Switzerland).

Microtissue Loading

The chip was filled with prewarmed (37 °C) Krebs–Ringer–Hepes Buffer (KRHB—131 × 10^{-3} M NaCl, 4.8 × 10^{-3} M KCl, 1.3 × 10^{-3} M CaCl2, 25 × 10^{-3} M Hepes, 1.2 × 10^{-3} M Kh2PO4, 1.2 × 10^{-3} M MgSO4, 0.5% bovine serum albumin). The microtissues were aspirated from an Akura 96 plate (InSphero AG, Schlieren, Switzerland) with a pipette and loaded into the chip via contact transfer with the pipette tip. The drop height was adjusted to 800 μm prior to each experiment. The height was defined as the distance between the PDMS rim structure of the chip and the center of the microtissue.

Experimental Setup and Perifusion System

The chip was placed on a microscope (DMI6000B, Leica Microsystems, Germany) and covered with a stage-top incubator (The Brick, Life Imaging Services, Basel Switzerland) to ensure >95% humidity and 5% CO_2. A liquid reservoir on the chip holder and a wet cotton pad at the bottom of the OmniTrayBox increased the humidity to minimize evaporation. Temperature was kept at 37 °C by an environmental box (The Cube, Life Imaging Services, Basel, Switzerland).

Syringe pumps (neMESYS, Cetoni GmbH, Korbussen, Germany) were connected to the inlet of the chip (Figure 2b). Polytetrafluoroethylene tubing (ID 0.3 mm, OD 0.6 mm, Bola GmbH, Grünsfeld, Germany) and metal connecting pieces, obtained from standard luer lock syringe-tubing connectors (22 GA ½” Bent 90 Deg, APM Technica AG, Heerbrugg, Switzerland), were connected together by short flexible silicone tubing (Tygon R3607, ID 0.25 mm, wall 0.91 mm, Idex Health & Science GmbH, Wertheim, Germany). A flow splitter enabled the connection of multiple syringes to a single inlet of the hanging-drop chip and a heatable perifusion cannula (PH01&TC02, Multichannel Systems, Reutlingen, Germany) ensured a constant temperature of 37 °C of the infused medium.

A peristaltic pump (peRISYS-S, Cetoni GmbH) was connected in the same way to the outlet of the microfluidic chip. Peristaltic tubing (Tygon S3 E-LFL, ID 0.27 mm, wall 0.91 mm, Idex Health & Science GmbH) was used for the peristaltic pump.

The final part of the tubing was attached to the sampling arm of the rotAXYS system (Cetoni GmbH) using fluid connectors (Upchurch Scientific Products, Oak Harbor, USA). A needle (facet cut, 0.15 mm ID, 0.3 mm OD, 16 mm length, Unimed, Lausanne, Switzerland) was connected at the end of the sampling tubing. All tubing was filled with medium before being connected to the chip.

Inflow rates of the syringe pumps were set to 15 μL min^{-1} and controlled by YouScope software[73] (Version: R2016-03). By monitoring the *z*-position of the center of the microtissue, an integrated feedback pump controller continuously adjusted the inflow rate to maintain the drop at its initial height. The peristaltic pump withdrew medium from the outlet at a constant rate of 15 μL min^{-1}. At this rate and with the tubing length, liquid reached the islet microtissue in the hanging-drop with a 4 min delay when switching between the different buffer solutions. This delay was corrected for in all graphs so that the time started when the medium reached the islet.

Automated Sampling

A programmable positioning and sampling system (rotAXYS, Cetoni GmbH) was used to collect outflow samples in predefined time intervals of down to 30 s. The Qmix Elements Software (Cetoni GmbH) was used to create a sampling script. An insulating Styrofoam box was placed underneath the sampling arm and filled with dry ice to cool down and freeze the samples. A multiwell plate (384-well, V-bottom, polypropylene, Thermo Fisher Scientific, USA) was sealed with a plate sealing foil (Platesealer EasySeal, Greiner Bio-One, Frickenhausen, Germany) inserted into the Styrofoam box and used for collecting the samples. With the defined flow rate of 15 μL min^{-1}, sampling volumes were at least 7.5 μL. The plates were stored and kept at −20 °C until analysis.

Microfluidic Characterization

The microfluidic hanging-drop chip was validated using a fluorescent Rhodamine 6G solution (Sigma-Aldrich, Buchs, Switzerland) at a concentration of 50 mg L^{-1}. DI water was first perfused at a flow rate of 15 μL min^{-1} for 60 min, then, the fluorescent dye was introduced into the chip at the same flow rate. The withdrawal flow rate at the outlet was set to 15 μL min^{-1}. Fluorescence within the hanging-drop was tracked over time by taking fluorescence images (GFP channel) every 10 s. Fluorescence in the central drop region around a glass bead was analyzed using ImageJ. A glass bead of similar size was used instead of an islet microtissue for drop-height regulation in the validation experiments.

Static GSIS and Quantification of Insulin and ATP

In order to prepare the islet microtissues for static GSIS, culture medium was removed and islet microtissues were washed twice with 70 μL KRHB containing 2.8×10^{-3} M glucose and equilibrated for 1 h in the same solution. GSIS was performed in the Akura 96 well-plate in 50 μL KRHB containing different glucose concentrations during 2 h. The supernatant was collected for ELISA analysis. After GSIS, the tissues were lysed to analyze total ATP content using CellTiter-Glo Luminescent Cell Viability Assay (Promega, with protease inhibitor cocktail (Promega, G6521)) and a microplate reader (Infinite M1000, TECAN, Switzerland). The lysates were then used for assessment of total insulin content.

After proper dilutions in KRHB were performed, total and secreted insulin was quantified using Stellux Chemi Human Insulin ELISA (Alpco, 80-INSHU-CH10).

Perifusion GSIS

In order to prepare the islet microtissues for FlowGSIS, they were transferred to a special preconditioning medium (hIsPCM, InSphero AG, Schlieren, Switzerland) 12 h before the experiment. A 100×10^{-6} M exendin-4 stock solution and 25×10^{-3} M tolbutamide in DMSO were diluted in KRHB shortly before experiments. Four 2.5 mL glass syringes were loaded with 2.8×10^{-3} M glucose + 0.1% DMSO (control), 16.7×10^{-3} M glucose + 0.1% DMSO (control), 2.8×10^{-3} M glucose + compound (100×10^{-9} M exendin-4 or 25×10^{-6} M tolbutamide), and 16.7×10^{-3} M glucose + compound (100×10^{-9} M exendin-4 or 25×10^{-6} M tolbutamide). These buffers were consecutively perfused through the hanging-drop in the following order; 90 min 2.8×10^{-3} M glucose + 0.1% DMSO for equilibration, 30 min 2.8×10^{-3} M glucose + compound (100×10^{-9} M exendin-4 or 25×10^{-6} M tolbutamide) for compound baseline secretion, 60 min 16.7×10^{-3} M glucose + compound (100×10^{-9} M exendin-4 or 25×10^{-6} M tolbutamide) for compound stimulation secretion, and 70 min with 2.8×10^{-3} M glucose + compound (100×10^{-9} M exendin-4 or 25×10^{-6} M tolbutamide) for post-GSIS secretion.

Data Analysis

For each given sampling interval, the average insulin secretion rate per microtissue (fmol IEQ^{-1} min^{-1}) was calculated from the known flow rate and the insulin concentration in the sample. To ensure that experiments were comparable, this value was normalized to islet microtissue size in IEQs, with one IEQ corresponding to the volume of a sphere with a diameter of 150 μm, yielding the secretion rate in (fmol IEQ^{-1} min^{-1}).

Microscopy During FlowGSIS

Throughout the 250 min of FlowGSIS, islet microtissues were continuously monitored with an inverted wide-field microscope (Leica DMI6000, Leica Microsystems, Switzerland) using a 10x objective and a 0.70x c-mount. Bright-field and fluorescence images were taken with a Leica DFC 340FX CCD camera. A mercury arc lamp was used as a light source for fluorescence imaging.

Immunofluorescence Microscopy

Primary antibodies; guinea pig polyclonal anti-insulin (Dako-Agilent, Santa Clara, USA), rabbit polyclonal anti-somatostatin (Dako-Agilent, Santa Clara, USA), mouse monoclonal anti-glucagon (Sigma-Aldrich, Buchs, Switzerland), and secondary antibodies; and donkey Fluorescein anti-guinea pig, donkey Cy3 anti-mouse, and donkey Cy5 anti rabbit (Jackson ImmunoResearch Laboratories, West Grove, PA, USA) were obtained commercially and used at dilutions recommended by the manufacturer. Native islets, dispersed islet cells, or islet microtissues were embedded into 2% agarose, which later was used for paraffin embedding. The samples were processed with microtome sectioning (5 μm). After de-paraffinization, the sections were permeabilized with 0.3% Triton X-100 in phosphate-buffered saline (PBS) and were blocked for 20 min with blocking solution (1% bovine

serum albumin, 3% guinea pig serum, and 3% donkey serum in PBS). Samples were incubated for overnight at 4 °C with primary antibodies in blocking solution. After three washing steps, secondary antibody and Hoechst solution (1:5000) were added in blocking solution at room temperature for 1 h at dark. Subsequently, the sections were washed and mounted with Hydromount medium (National Diagnostics, Atlanta, GA, USA). The fluorescent images of the islets were acquired with an inverted wide-field microscope (Leica DMi8 Microscope, DFC 9000 GT Camera, Leica Microsystems, Switzerland) using a 20x dry objective.

Diffusion-Convection Transport Model

Diffusive-convective transport of molecules through the liquid phase and PDMS was modeled numerically using the finite-element method. Dimensions of the chip and drops were reproduced in COMSOL Multiphysics software (COMSOL AB, Stockholm, Sweden).

The fluid dynamics model included the viscosity and density of the medium at 37 °C, which were assumed to be identical to water. Slip and no-slip boundary conditions were assumed at the liquid–air and liquid–PDMS interfaces, respectively. A constant flow of 15 μL min^{-1} and a null pressure were assumed at the inlet and outlet boundaries, respectively. A logarithm scale color mapping of the resulting flow was incorporated in Figure 2b, showing that flow speed at the islet site was significantly lower than in the channel, which reduced shear stress while direct molecule transport was enabled. These data were used to model the convective transport of molecules.

The diffusion-convection model was applied for Rhodamine 6G and insulin with diffusion coefficients of 4.14×10^{-10} m^2 s^{-1}[74,75] and 1.5×10^{-10} m^2 s^{-1},[71] respectively. From the determined diffusion coefficient at 25°C, its value was derived at 37 °C using the Stokes–Einstein equation, and the viscosity of water. The diffusion coefficient in PDMS and the water/PDMS partition coefficient of Rhodamine 6G were 2.08×10^{-13} m^2 s^{-1} and 89.[76] For the case of Rhodamine 6G (Figure 2c), a normalized concentration influx was applied at the inlet and both, the average concentration in the entire hanging-drop and at the islet, were computed over time. For the case of insulin (Figure 2d), a short insulin secretion burst from an islet was simulated. The values were taken from a measurement (Figure 3a) and a total release of 2.5 fmol IEQ^{-1} insulin within one burst was simulated, and a fast secretion within 1 s was assumed, such that the secretion averaged 5 fmol IEQ^{-1} min^{-1} over one sampling interval of 30 s. The concentration at the outlet was probed over time to investigate sampling aliasing due to various boundary conditions at the liquid–air interface (Movie S3, Supporting Information).

Supplementary Material

Refer to Web version on PubMed Central for supplementary material.

Acknowledgements

P.M.M. and B.Y. contributed equally to this work. This work was financially supported by the Swiss Commission for Technology and Innovation (CTI) (Grant No. 18024.1 PFLS-LS), the Swiss National Science Foundation (SNF 2-77079-16 Infected body-on-chip), and the European Commission (Grant No. 668350 LSFM4LIFE).

References

[1]. In't Veld, P, Marichal, M. The Islets of Langerhans. Islam, MS, editor. Springer; Netherlands, Dordrecht: 2010. 1–19.

[2]. Bell GI, Polonsky KS. Nature. 2001; 414:788. [PubMed: 11742410]

[3]. Seino S, Shibasaki T, Minami K. J Clin Invest. 2011; 121:2118. [PubMed: 21633180]

[4]. Satin LS, Butler PC, Ha J, Sherman AS. Mol Aspects Med. 2015; 42:61. [PubMed: 25637831]

[5]. Michael MD, Kulkarni RN, Postic C, Previs SF, Shulman GI, Magnuson MA, Kahn CR. Mol Cell. 2000; 6:87. [PubMed: 10949030]

[6]. Abdulreda M, Fachado A, Molina J, Rodriguez-Diaz R, Jacques-Silva MC, Cabrera O, Abdulreda MH, Berggren PO, Caicedo A. Protoc Exch. 2011; :260.doi: 10.1038/protex.2011

[7]. Ahrén B. Diabetologia. 2000; 43:393. [PubMed: 10819232]

[8]. Rutter GA, Hodson DJ. MolEndocrinol. 2013; 27:1984.

[9]. Pedersen MG, Bertram R, Sherman A. Biophys J. 2005; 89:107. [PubMed: 15834002]

[10]. El-Ali J, Sorger PK, Jensen KF. Nature. 2006; 442:403. [PubMed: 16871208]

[11]. Dittrich PS, Manz A. Nat Rev Drug Discovery. 2006; 5:210. [PubMed: 16518374]

[12]. Kovarik ML, Gach PC, Ornoff DM, Wang Y, Balowski J, Farrag L, Allbritton NL. Anal Chem. 2012; 84:516. [PubMed: 21967743]

[13]. Rocheleau JV, Walker GM, Head WS, McGuinness OP, Piston DW. Proc Natl Acad Sci USA. 2004; 101:12899. [PubMed: 15317941]

[14]. Nourmohammadzadeh M, Xing Y, Lee JW, Bochenek MA, Mendoza-Elias JE, McGarrigle JJ, Marchese E, Chun-Chieh Y, Eddington DT, Oberholzer J, Wang Y. Lab Chip. 2016; 16:1466. [PubMed: 26999734]

[15]. Brooks JC, Ford KI, Holder DH, Holtan MD, Easley CJ. Analyst. 2016; 141:5714. [PubMed: 27486597]

[16]. Heileman K, Daoud J, Hasilo C, Gasparrini M, Paraskevas S, Tabrizian M. Biomicrofluidics. 2015; 9

[17]. Godwin LA, Pilkerton ME, Deal KS, Wanders D, Judd RL, Easley CJ. AnalChem. 2011; 83:7166.

[18]. Shackman JG, Reid KR, Dugan CE, Kennedy RT. Anal Bio anal Chem. 2012; 402:2797.

[19]. Adewola AF, Lee D, Harvat T, Mohammed J, Eddington DT, Oberholzer J, Wang Y. Biomed Microdevices. 2010; 12:409. [PubMed: 20300858]

[20]. Mohammed JS, Wang Y, Harvat TA, Oberholzer J, Eddington DT. Lab Chip. 2009; 9:97. [PubMed: 19209341]

[21]. Lenguito G, Chaimov D, Weitz JR, Rodriguez-Diaz R, Rawal SAK, Tamayo-Garcia A, Caicedo A, Stabler CL, Buchwald P, Agarwal A. Lab Chip. 2017; 17:772. [PubMed: 28157238]

[22]. Cabrera O, Jacques-Silva MC, Berman DM, Fachado A, Echeverri F, Poo R, Khan A, Kenyon NS, Ricordi C, Berggren PO, Caicedo A. Cell Transplant. 2007; 16:1039. [PubMed: 28866924]

[23]. Dishinger JF, Reid KR, Kennedy RT. Anal Chem. 2009; 81:3119. [PubMed: 19364142]

[24]. Dishinger JF, Kennedy RT. Anal Chem. 2007; 79:947. [PubMed: 17263320]

[25]. Nunemaker CS, Dishinger JF, Dula SB, Wu R, Merrins MJ, Reid KR, Sherman A, Kennedy RT, Satin LS. PLoS One. 2009; 4:e8428. [PubMed: 20037650]

[26]. Ritzel RA, Veldhuis JD, Butler PC. J Clin Endocrinol Metab. 2003; 88:742. [PubMed: 12574208]

[27]. Yi L, Wang X, Dhumpa R, Schrell AM, Mukhitov N, Roper MG. Lab Chip. 2015; 15:823. [PubMed: 25474044]

[28]. Roper MG, Shackman JG, Dahlgren GM, Kennedy RT. Anal Chem. 2003; 75:4711. [PubMed: 14674445]

[29]. Shackman JG, Dahlgren GM, Peters JL, Kennedy RT. Lab Chip. 2005; 5:56. [PubMed: 15616741]

[30]. Bandak B, Yi L, Roper MG. Lab Chip. 2018; 18:2873. [PubMed: 30109329]

[31]. Buchwald P, Wang X, Khan A, Bernal A, Fraker C, Inverardi L, Ricordi C. Cell Transplant. 2009; 18:1223. [PubMed: 19818209]

[32]. Brissova M, Fowler MJ, Nicholson WE, Chu A, Hirshberg B, Harlan DM, Powers AC. J Histochem Cytochem. 2005; 53:1087. [PubMed: 15923354]

[33]. Wang X, Misawa R, Zielinski MC, Cowen P, Jo J, Periwal V, Ricordi C, Khan A, Szust J, Shen J, Millis JM, et al. PLoS One. 2013; 8:e67454. [PubMed: 23826303]

[34]. Harata M, Liu S, Promes JA, Burand AJ, Ankrum JA, Imai Y. Physiol Rep. 2018; 6:e13907. [PubMed: 30370689]

[35]. Yu Y, Gamble A, Pawlick R, Pepper AR, Salama B, Toms D, Razian G, Ellis C, Bruni A, Gala-Lopez B, (Lulu) Lu J, et al. Diabetologia. 2018; 61:2016. [PubMed: 29971529]

[36]. Hopcroft DW, Mason DR, Scott RS. In Vitro Cell Dev Biol. 1985; 21:421. [PubMed: 3897182]

[37]. Halban PA, Powers SL, George KL, Bonner-Weir S. Diabetes. 1987; 36:783. [PubMed: 3556277]

[38]. Zuellig RA, Cavallari G, Gerber P, Tschopp O, Spinas GA, Moritz W, Lehmann R. J Tissue Eng Regener Med. 2017; 11:109.

[39]. Frey O, Misun PM, Fluri DA, Hengstler JG, Hierlemann A. Nat Commun. 2014; 5

[40]. de Groot TE, Veserat KS, Berthier E, Beebe DJ, Theberge AB. Lab Chip. 2016; 16:334. [PubMed: 26660268]

[41]. Frey O, Misun PM, Fluri DA, Hengstler JG, Hierlemann A. Nat Commun. 2014; 5

[42]. Birchler A, Berger M, Jäggin V, Lopes T, Etzrodt M, Misun PM, Pena-Francesch M, Schroeder T, Hierlemann A, Frey O. Anal Chem. 2016; 88:1222. [PubMed: 26694967]

[43]. Boos JA, Misun PM, Michlmayr A, Hierlemann A, Frey O. Adv Sci. 2019; 6

[44]. Misun PM, Rothe J, Schmid YRF, Hierlemann A, Frey O. Microsyst Nanoeng. 2016; 2

[45]. Rismani Yazdi S, Shadmani A, Bürgel SC, Misun PM, Hierlemann A, Frey O. Lab Chip. 2015; 75:4138.

[46]. Ichii H, Sakuma Y, Pileggi A, Fraker C, Alvarez A, Montelongo J, Szust J, Khan A, Inverardi L, Naziruddin B, Levy MF, et al. Am J Transplant. 2007; 7:1010. [PubMed: 17391141]

[47]. Kin T, Senior P, O'Gorman D, Richer B, Salam A, Shapiro AMJ. Transpl Int. 2008; 27:1029.

[48]. Kuo CY, Herrod HG, Burghen GA. Pancreas. 1992; 7:320. [PubMed: 1375749]

[49]. Matta SG, Wobken JD, Williams FG, Bauer GE. Pancreas. 1994; 9:439. [PubMed: 7937692]

[50]. Shizuru J, Trager D, Merrell RC. Diabetes. 1985; 34:898. [PubMed: 3161769]

[51]. Wolf-Jochim M, Wöhrle M, Federlin K, Bretzel RG. Exp Clin Endocrinol Diabetes. 1995; 703:118.

[52]. Tze WJ, Tai J. Transplantation. 1984; 38:107. [PubMed: 6431662]

[53]. Cabrera O, Berman DM, Kenyon NS, Ricordi C, Berggren PO, Caicedo A. Proc Natl Acad Sci USA. 2006; 703:2334.

[54]. Auner AW, Tasneem KM, Markov DA, McCawley LJ, Hutson MS. Lab Chip. 2019; 79:864.

[55]. Hou JC, Min L, Pessin JE. Vitam Horm. 2009; 80:473. [PubMed: 19251047]

[56]. Sola D, Rossi L, Schianca GPC, Maffioli P, Bigliocca M, Mella R, Corlianò F, Fra GP, Bartoli E, Derosa G. Arch Med Sci. 2015; 4:840.

[57]. Proks P, Reimann F, Green N, Gribble F, Ashcroft F. Diabetes. 2002; 57:S368.

[58]. Doyle ME, Egan JM. Pharmacol Ther. 2007; 113:546. [PubMed: 17306374]

[59]. Lovshin JA, Drucker DJ. Nat Rev Endocrinol. 2009; 5:262. [PubMed: 19444259]

[60]. Briatore L, Salani B, Andraghetti G, Danovaro C, Sferrazzo E, Scopinaro N, Adami GF, Maggi D, Cordera R. Obesity. 2008; 76:77.

[61]. Steiner KE, Mouton SM, Bowles CR, Williams PE, Cherrington AD. Diabetes. 1982; 37:964.

[62]. Gerich JE. Diabetes. 2002; 57:S117.

[63]. Fritsche A, Stefan N, Hardt E, Schützenauer S, Häring H, Stumvoll M. Eur J Clin Invest. 2000; 30:411. [PubMed: 10809901]

[64]. Hauge-Evans AC, King AJ, Carmignac D, Richardson CC, Robinson ICAF, Low MJ, Christie MR, Persaud SJ, Jones PM. Diabetes. 2009; 58:403. [PubMed: 18984743]

[65]. Derosa G, Maffioli P. Curr Clin Pharmacol. 2012; 7:214. [PubMed: 22432846]

[66]. Toepke MW, Beebe DJ. Lab Chip. 2006; 6:1484. [PubMed: 17203151]

[67]. Ohta M, Nelson D, Nelson J, Meglasson MD, Erecinska M. J Biol Chem. 1990; 265:17525. [PubMed: 2211646]

[68]. Dionne KE, Colton CK, Yarmush ML. Biotechnol Prog. 1991; 7:359. [PubMed: 1367346]

[69]. Nourmohammadzadeh M, Lo JF, Bochenek M, Mendoza-Elias JE, Wang Q, Li Z, Zeng L, Qi M, Eddington DT, Oberholzer J, Wang Y. Anal Chem. 2013; 85:11240. [PubMed: 24083835]

[70]. Lo JF, Wang Y, Blake A, Yu G, Harvat TA, Jeon H, Oberholzer J, Eddington DT. Anal Chem. 2012; 84:1987. [PubMed: 22296179]

[71]. Buchwald P. Biol Med Model. 2011; 8:20.

[72]. Misun, PM, Birchler, AK, Lang, M, Hierlemann, A, Frey, O. Methods Mol Biol. Ertl, P, Rothbauer, M, editors. Springer, NY; 2018. 183–202.

[73]. Lang M, Rudolf F, Stelling J. Curr Protoc Mol Biol. 2012; 74

[74]. Kapusta, P. Application Note. PicoQuant GmbH; Berlin: 2010.

[75]. Müller CB, Loman A, Pacheco V, Koberling F, Willbold D, Richtering W, Enderlein J. Europhys Lett. 2008; 83:46001.

[76]. Adiraj Iyer M, Eddington DT. Lab Chip. 2019; 79:574.

Europe PMC Funders Author Manuscripts

Europe PMC Funders Author Manuscripts

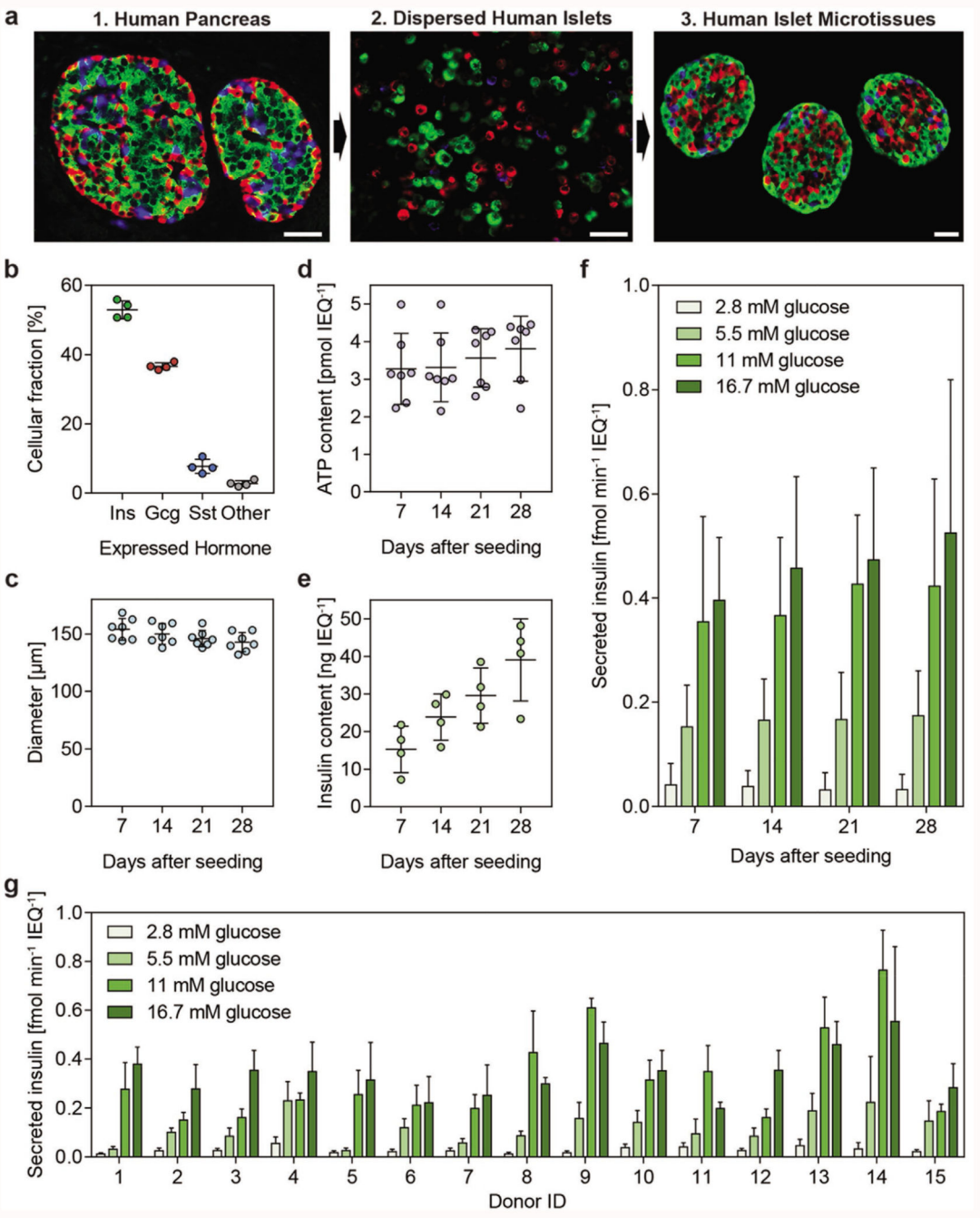

Figure 1. Characterization of reaggregated islet microtissues.

a) Stages of islet microtissue production displayed through immunofluorescence staining for insulin (β-cells, green), glucagon (α-cells, red), and somatostatin (δ-cells, blue). Images show (1) native islets in the human pancreas, (2) dissociated islets, and (3) islet microtissues. Scale bar: 100 µm. b) Endocrine-cell compositions of the islet microtissues were calculated from morphometric analysis of the microtissue sections from four individual donors. c) Cross-sectional diameter, d) total ATP content, e) total insulin content, and f) GSIS of human islet microtissues were assessed on days 7, 14, 21, and 28 post production. g)

Glucose-stimulated insulin secretion of islet microtissues from 15 different donors 7 d post production is shown. ATP content, insulin content, and secreted insulin were normalized to the islet size in islet equivalents (IEQs), which refer to an islet with 150 μm diameter. Data in panels (c), (d), and (f) have been obtained from islets of seven individual donors, while panel (e) includes data of islets from four individual donors, mean ± standard deviations.

Europe PMC Funders Author Manuscripts

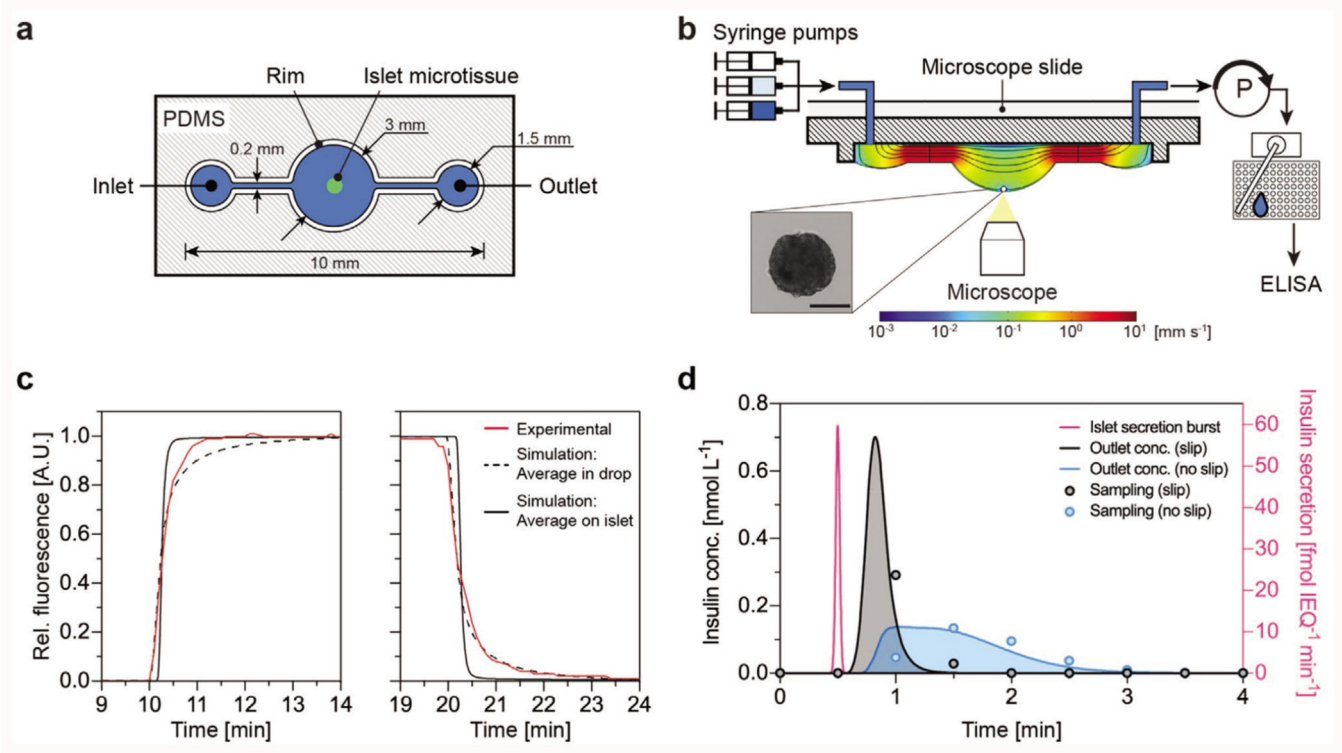

Figure 2. Microfluidic hanging-drop device and flow characteristics.

a) Top view of the hanging-drop chip hosting the microtissue. b) Microfluidic perifusion setup and schematic cross-sectional view along the hanging-drop chip. The microtissue is located at the bottom of the hanging-drop. Syringes are connected to the inlet of the chip, and a peristaltic pump is actively withdrawing the medium from the outlet. An automated sampling system collects the medium in a 384-well plate for down-stream ELISA. Scale bar: 100 μm. c) Experimental measurements and simulation of the concentration changes in the hanging-drop. Experimental data (red) of the average relative fluorescence in the hanging-drop upon switching from deionized water to Rhodamine 6G solution (left), and back to deionized water (right). A simulation shows the average concentration in the drop (dotted black) and the average concentration around the islet microtissue (black). d) Modeling result of the insulin concentration at the chip outlet following a sharp 1-s wide insulin secretion burst (purple) at the islet with a total release of 2.5 fmol IEQ^{-1} insulin. The resulting outlet concentration has been calculated assuming either a slip (black) or a no-slip (blue) boundary condition at the liquid–air surface. The resulting experimental data points are shown for a sampling rate of two samples per minute.

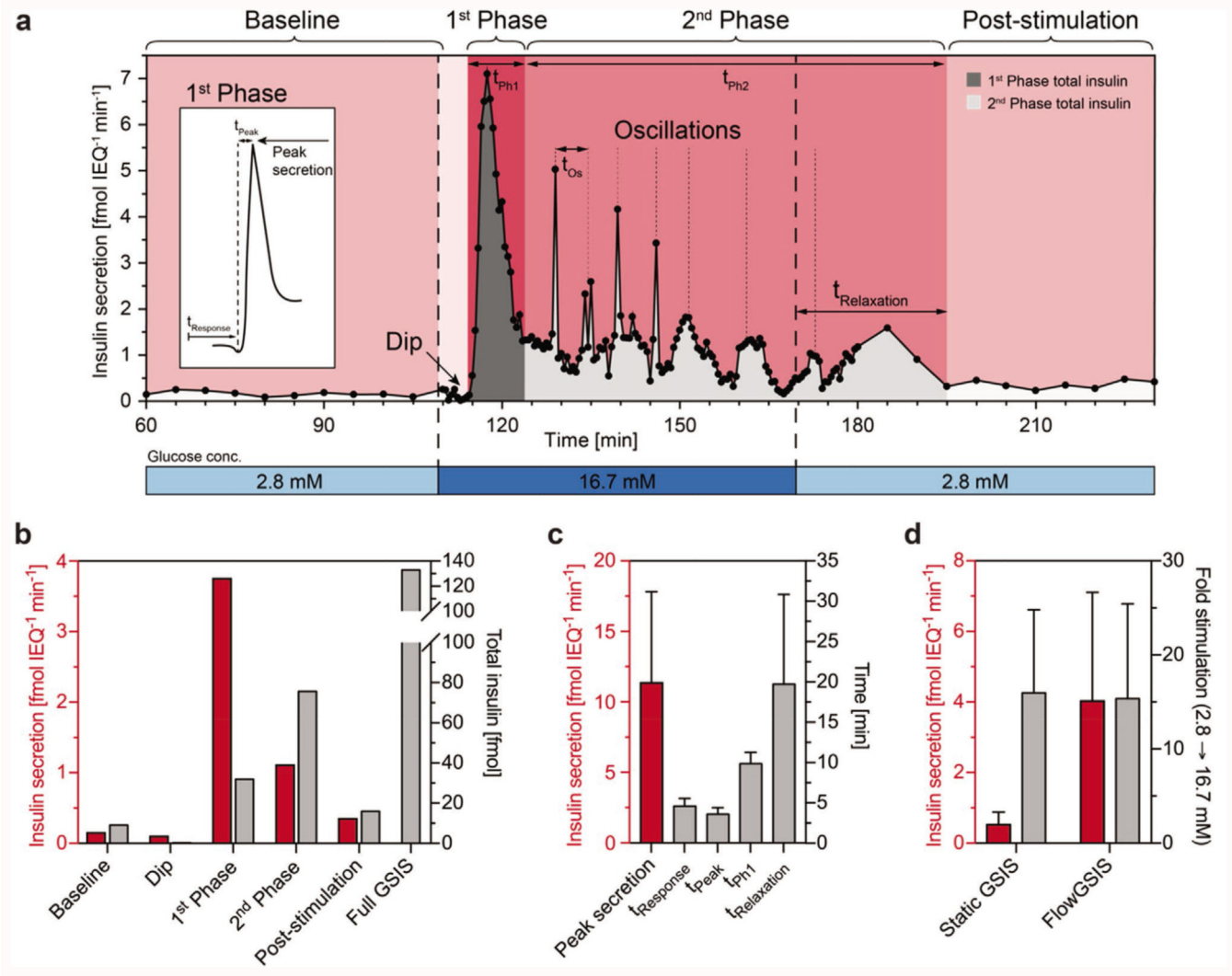

Figure 3.

a) High-resolution microfluidic FlowGSIS measurement of a single human islet microtissue. A change from low (2.8×10^{-3} M) to high (16.7×10^{-3} M) glucose concentrations stimulates insulin secretion in a bi-phasic pattern. Samples were continuously taken every 5 min during low glucose conditions (60–110 min and 180–230 min) and every 30 s in the high-glucose phase (110–180 min). Islets secreted insulin at a low level in a stable, nonoscillatory pattern at low glucose concentrations (basal secretion). High glucose concentrations induced highly dynamic insulin secretion with a dip at the beginning, a prominent first phase, which was followed by a sustained, pulsatile second phase. The inset shows the characteristic shape of the first secretion peak and the parameters that can be extracted from the curve. b) Insulin secretion rate (red) and the total secreted insulin (gray) in each phase of the FlowGSIS are represented in panel (a). c) Characteristic timing of insulin release (gray) and the maximum secretion rate in the first phase (red) ($n = 7$ islets from four different donors). d) Flow-induced increase of insulin secretion (red) and the respective stimulation-level factor from baseline to high glucose (gray), static GSIS ($n = 9$ donors), FlowGSIS ($n = 5$ donors). Data represent mean ± standard deviations.

Europe PMC Funders Author Manuscripts

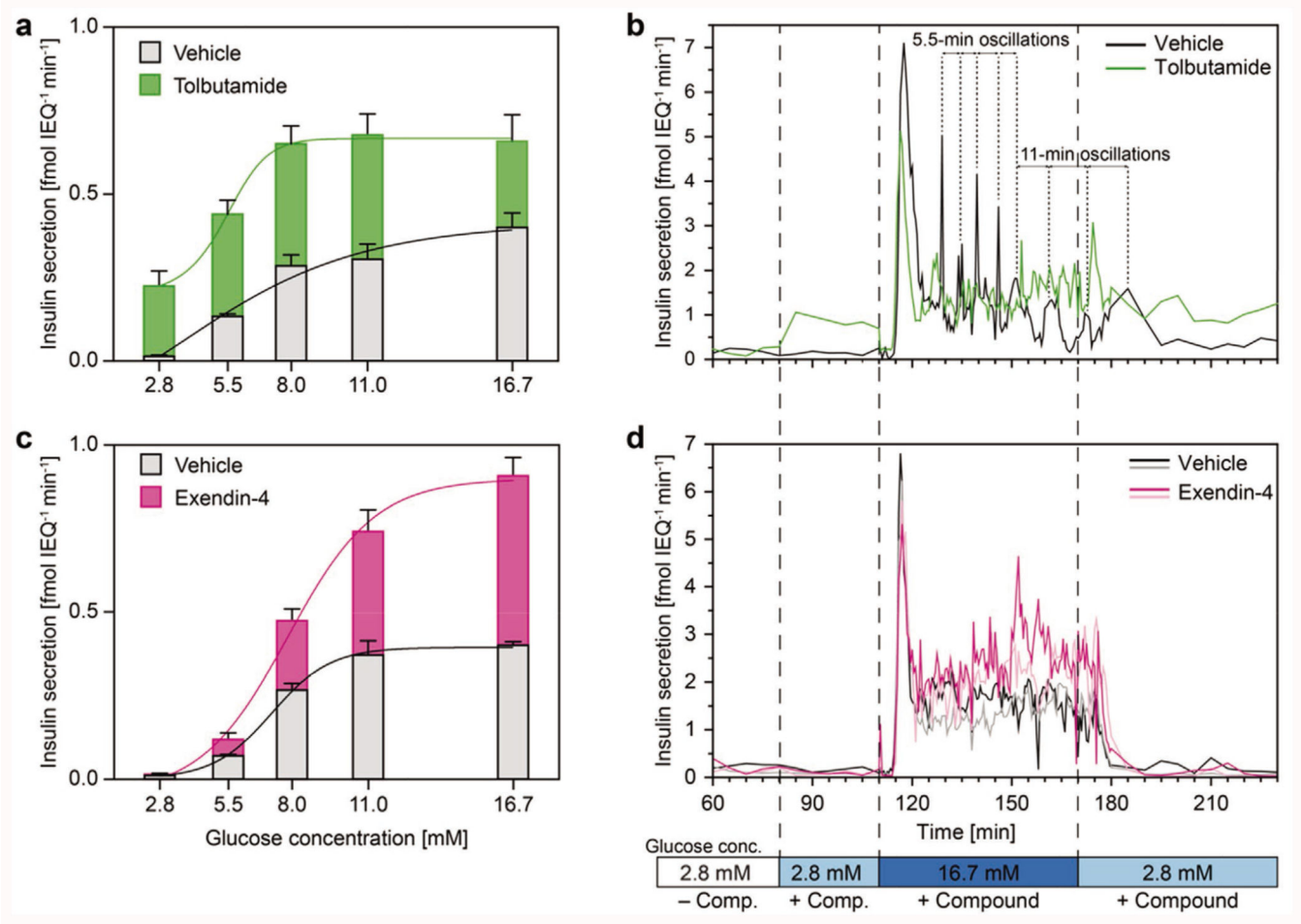

Figure 4. Static well plate and high-resolution FlowGSIS experiments on single human islet microtissues.

The secretion of insulin was stimulated with different glucose concentrations ranging from 2.8×10^{-3} M up to 16.7×10^{-3} M. a) Insulin secretion under static conditions with 25×10^{-6} M tolbutamide (green, $n = 5$ islets for each condition) and c) 100×10^{-9} M exendin-4 (red, $n = 6$ islets for each condition). b) Resolving the insulin secretion dynamics by using single islets treated with tolbutamide (green) and d) exendin-4 (purple). More FlowGSIS measurements for tolbutamide (different donors) are shown in Figure S7 (Supporting Information). Islets from two different donors were used (Donor A for tolbutamide and Donor D for exendin-4), and the measurements were compared to control islets from the same donor without compound (black and gray). More details are shown in Figures S5 and S6 (Supporting Information). The highly dynamic biphasic insulin secretion with a prominent first phase and a sustained, pulsatile second phase was detected under all conditions. Data obtained under static conditions represent mean values ± standard deviations.

Europe PMC Funders Author Manuscripts

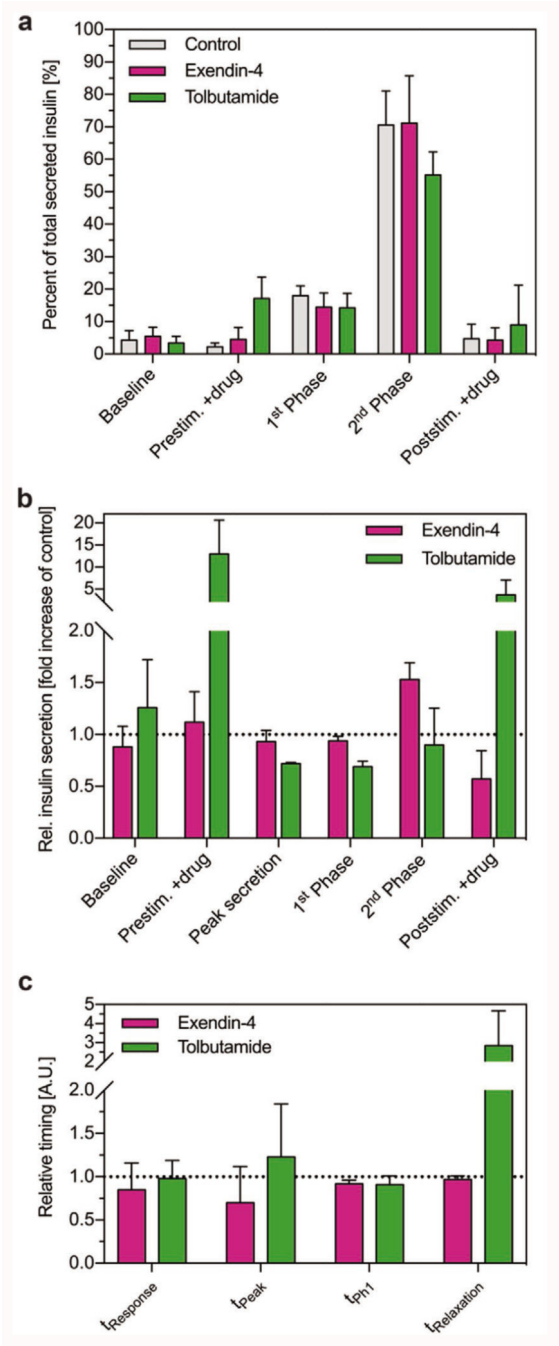

Figure 5. Effects of exendin-4 (red) and tolbutamide (green) on the dynamics of insulin secretion.

a) Distribution of insulin secretion in different phases of insulin release during FlowGSIS assays. The data represent the amount of insulin that was secreted in each phase relative to the total secreted insulin of the full FlowGSIS (control $n = 5$ islets; exendin-4 $n = 3$ islets; tolbutamide $n = 3$ islets). b) Effects of compounds on the secretion rate in different phases of GSIS. The data represent average insulin secretion rates during each phase of a FlowGSIS relative to the control of the same donor (exendin-4, $n = 2$ islets; tolbutamide, $n = 3$ islets). c) Effects of compounds on the average timing of insulin release relative to the control of the

same donor (exendin-4, $n = 2$ donors; tolbutamide, $n = 3$ donors). Data represent mean values ± standard deviations.

Europe PMC Funders Author Manuscripts

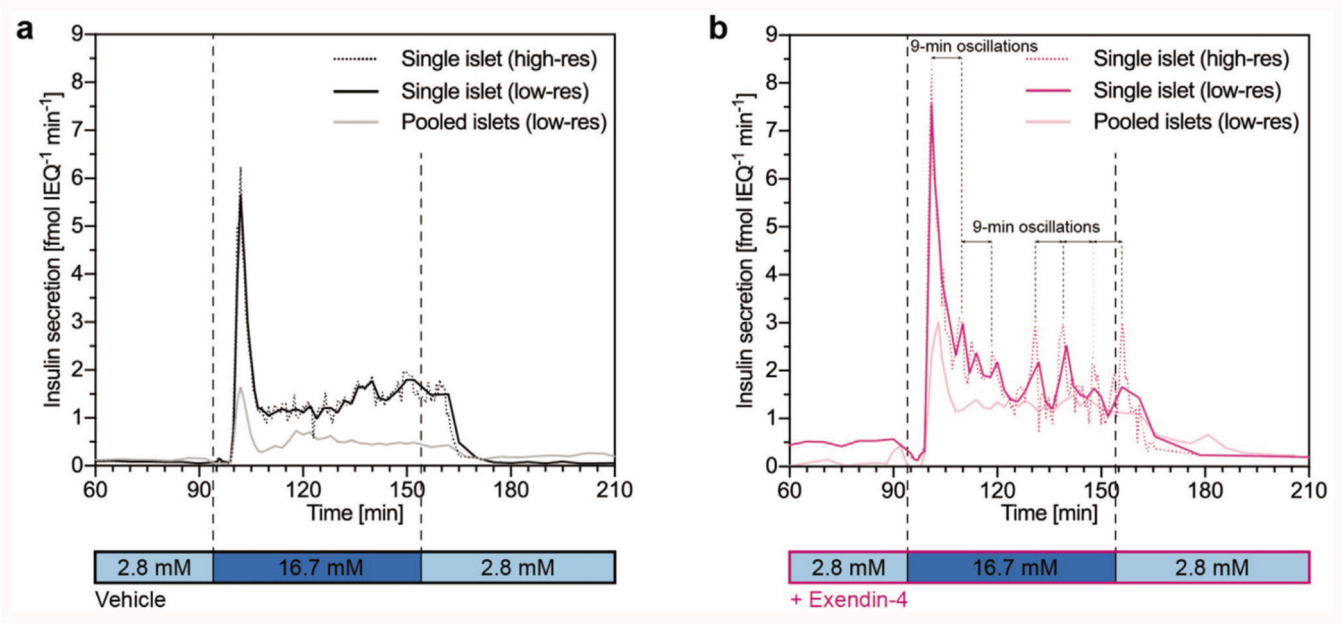

Figure 6.

FlowGSIS with single islets versus three to four pooled islets for a) control GSIS and b) GSIS with dosage of exendin-4. A switch from low (2.8×10^{-3} M) to high (16.7×10^{-3} M) glucose concentrations induced highly dynamic insulin secretion in a bi-phasic manner with a dip at the beginning, a prominent first phase, which was followed by a sustained, pulsatile second phase. GSIS with single islets showed higher insulin secretion rates compared to pooled islets under both conditions. Exendin-4 stimulated insulin secretion in the first and second phases for both single islets and pooled islets, compared to the vehicle control. Samples were taken every 5 min between 60–95 min and 165–210 min, every 30 s for the high-resolution sampling (single islet), and every 2 min for the low-resolution sampling (pooled islets) during the high-glucose phase (95–165 min). Data for the “single islet low-resolution” condition were calculated from the “single islet high-resolution” data by averaging four sampling points to show effects of high (30 s) versus low (2 min) resolution sampling and to compare with the “pooled-islet low-resolution” condition. Islets from two different donors were used for the GSIS in the vehicle control (a) and islets from a single donor were used for the GSIS with exendin-4 (b).